IEEE Access
Multidisciplinary | Rapid Review | Open Access Journal

Received 1 March 2023, accepted 5 April 2023, date of publication 17 April 2023, date of current version 27 April 2023.

Digital Object Identifier 10.1109/ACCESS.2023.3267808

RESEARCH ARTICLE

Closed Form Approximations for UAV Line-of-Sight Probability in Urban Environments

IMRAN MOHAMMED, (Student Member, IEEE), SWAROOP GOPALAM, (Member, IEEE), IAIN B. COLLINGS, (Fellow, IEEE), AND STEPHEN V. HANLY, (Fellow, IEEE)
School of Engineering, Macquarie University, Sydney, NSW 2109, Australia

Corresponding author: Stephen V. Hanly (stephen.hanly@mq.edu.au)

This work was supported by the Australian Research Council Discovery Project under Grant DP200101627.

ABSTRACT This paper presents a new approach to estimate the probability of line-of-sight (LoS) for unmanned aerial vehicle (UAV) communications. We provide lower and upper bounds on the probability of LoS in terms of what we call the first-building-LoS probability. We provide a statistical model for the ground distance to the first building along the line from the user to the UAV. Based on this we provide a general formula for the first-building-LoS probability for urban environments where the building heights follow a Rayleigh distribution. We show that the first-building-LoS probability is a good estimate for the probability of LoS. Our closed-form formulas estimate the probability of LoS significantly more accurately than the existing approaches. We also obtain closed-form estimates of Area Line-of-Sight Probabilities for a scenario in which the UAV provides coverage to a circular region on the ground.

INDEX TERMS Aerial base stations, channel modelling, drones, probability of line of sight, UAV communications, unmanned aerial vehicles.

I. INTRODUCTION

Unmanned Aerial Vehicles (UAVs) (also known as drones) have been recently considered for use as aerial base stations. UAVs are expected to be a vital component of 5G and beyond 5G architectures [1]. UAVs can be used to enhance the existing terrestrial infrastructure when there is a high demand for communication services for a short period [1], [2], [3], e.g., UAVs can act as additional base stations for large gatherings such as sports events [4]. There is also a rise in UAV applications in non-military public safety scenarios [1], [3], [5], [6], e.g., UAVs can be rapidly deployed during disaster scenarios such as earthquakes, bush fires, floods, where the terrestrial communication infrastructure is affected [2], [7].

The large scale propagation characteristics for the UAV channel depend on whether the link (between the UAV and the ground user equipment (UE)) is Line-of-Sight (LoS) or not. Hence, a key aspect of UAV channel modelling is the calculation of the probability of LoS, which is defined as the probability that the direct-path between the UAV and UE is not blocked by any of the buildings. The probability of LoS is required in many UAV applications, including determining the optimal height and placement of a UAV, for an energy-efficient deployment of UAV, and for path-planning [6], [8], [9].

In this paper, we consider the problem of characterising the probability of LoS for a wide range of urban built environments. We derive a LoS probability expression which is more accurate than previous results, and which is valid for arbitrary Rayleigh building height distributions, arbitrary square building footprint sizes and street widths.

In the International Telecommunication Union Radiocommunication Sector (ITU-R) standard [10], [11], the probability of LoS for a given ground distance (distance between UAV and UE) and for a given UAV height was proposed. The probability of LoS was calculated assuming that buildings were evenly spaced along a line connecting the UAV and UE. Importantly though, that one-dimensional (1D) assumption only holds when the projection of the line connecting the UE and UAV on the ground is parallel to the direction of the streets. In general of course, the spacing of

The associate editor coordinating the review of this manuscript and approving it for publication was Zhenzhou Tang.

the buildings (along the LoS) depends on the orientation of the UAV and the UE with respect to the street grid in two dimensions, and moreover the buildings are not evenly spaced along that direction in general.

In [8] and [12], closed form expressions for probability of LoS as a function the elevation angle were provided for four specific urban environments. In [8], the function was obtained by curve-fitting the results of the 1D method in [11] for various elevation angles. In [12], a function was obtained by curve-fitting Monte-Carlo simulations for a two dimensional (2D) grid model. In each case, the results only applied to the specific scenarios that were considered, in terms of building heights, building footprint sizes, and street widths, and cannot be directly applied for other grid dimensions.

In contrast to the grid models, an alternative built model was considered in [13], [14], and [15], where the buildings were located on a 2D plane according to a homogeneous Poisson point process. In [13], the probability of LoS was derived assuming that all the building heights are equal. In [15], communication between two UAVs was considered. In each case, the Poisson point process model with restricted building height assumptions facilitated mathematical analysis, however it is not realistic, since in practical urban settings buildings are located in planned blocks with a grid structure. In [14], buildings were also located according to a spatial Poisson Point Process. In [16], the probability of LoS as a function of UAV height and ground distance was presented. It assumed that the building adjacent to the mobile in the direct path will be the dominant obstruction to radio propagation. It also made a simplifying assumption that the building height distribution is symmetrical around the mean, in order to facilitate their analysis. Their results are therefore not applicable to the practical building model in ITU-R [11], which is Rayleigh distributed, and therefore not symmetrical.

Many papers have used the probability of LoS models from [8], [11], [12], [13], [14], and [16] when addressing specific problems of UAV communications, including [6], [9], [15], [17], [18], [19], [20], [21], [22], [23], [24], [25], [26], [27], [28], [29], [30], [31], [32], [33], [34]. As such, they all suffer from the inaccuracy of those models, from either making 1D geographical approximations or assuming totally randomised building location models.

In [35], we presented a significantly more accurate probability of LoS model that can be applied to the specific problems in [6], [9], [15], [17], [18], [19], [20], [21], [22], [23], [24], [25], [26], [27], [28], [29], [30], [31], [32], [33], and [34]. We adopted the full 2D environment model from [11] and provided an accurate numerical approach to calculate the probability of LoS as a function of ground distance and UAV height for the four urban environments specified in [11], which had not been done before.

In [36], a 2D model was also considered for a UAV in a mm-wave setting, in which there was a fixed base station located in a street or intersection, and the UAV is placed above an arbitrary fixed position on the 2D street grid. Similar to our work [35], [37], they showed that the earlier 1D approaches based on [10] and [11] significantly overestimate the line of sight probability. The model in [36] differs from the standard one [10], [11] in that street locations are random, being governed by two independent Poisson point processes. Closed-form expressions for the probability of LoS to the fixed base station were obtained. They also showed how to compute an area line-of-sight probability, but did not provide a closed form expression for this quantity. In this paper, we focus on a different problem where the UAV is the base station communicating with randomly located UEs on the ground, and we provide closed-form expressions for the average probability of LoS for a UE at a fixed ground distance from the UAV.

In our previous work [35], we took a curve fitting approach, as in [8] and [12], which we applied to four scenarios identified in the ITU-R standard [10], [11], corresponding to specific choices for building footprint size, street width, and building height distribution. This approach can be extended to other scenarios, but time consuming numerical computations are required to curve fit to each particular scenario.

In this paper, we propose a fully 2D approach to the practical case of a rectangular street grid, and where the UAV can be uniformly randomly located at any orientation relative to the UE and the grid. We make an important observation that the probability of LoS is dominated by the building that is nearest to the UE along the direction towards the UAV. We derive the associated first-building-LoS-probability, and use it to provide two closed form expressions that accurately approximate the average probability of LoS function. Our expressions apply to a general urban environment with arbitrary parameters of building footprint size, street width, and Rayleigh building height distribution. This is in contrast to expressions derived in other works, such as [8], [12], and [35], that are restricted to particular settings of the building footprint size, street width, and building height distribution. Using Monte-Carlo simulations, we show that our results are much more accurate compared to existing methods.

In addition to considering homogeneous building distribution scenarios, it is also important to consider practical built landscapes, where the building distributions are in-homogeneous. For example, consider a UAV flying over high-rise buildings, communicating with UEs in a nearby suburban area. The buildings between the UAV and UE are a mixture of suburban and high-rise, with different height distributions. We show that our first-building-LoS probability expressions (derived for the homogeneous case) are also accurate in in-homogeneous environments. We provide the range of elevation angles and Rayleigh parameters for which our model is highly accurate.

Our contributions are as follows:

- We provide a lower and upper bound on the average probability of LoS for homogeneous building distributions. The bound is in terms of the first-building-LoS probability. We show that the first-building-LoS

probability is a good estimate for the average probability of LoS.

- We provide a statistical model for the distance to the first building along the line from the UE to the UAV.
- We then develop a novel method for calculating the first-building-LoS probability. Based on this we provide two closed-form estimates for the first-building-LoS probability that apply for all urban environments where the building heights follow a Rayleigh distribution. Our approach can be easily adapted for other building height distributions, i.e., it is not limited to the Rayleigh distribution.
- We provide the Monte-Carlo simulation results for the four urban environments that were considered in [11]. We compare the results with our method and others from the literature. We show that our closed-form formulas are much closer to the Monte-Carlo simulations.
- We provide a formula to compute the area probability of LoS, which is the average probability of LoS when the UE is randomly (uniformly) located in a cell of radius R around the UAV. We provide two closed-form approximation formulas for this quantity.
- We propose a practical inhomogeneous built environment, where the building height distribution changes with the building location on the 2D plane. Using a Monte-Carlo simulation, we show that our results are applicable in this inhomogeneous case, for a wide-range of elevation angles and building height parameters.

II. UAV OPERATING ENVIRONMENT PARAMETERS

An urban built environment is characterized by a two dimensional grid of buildings, as shown in Fig. 1. In the figure, the buildings are represented with light grey squares, and the white space between them are streets. The width of each building is denoted by w. The distance between the buildings (or the width of the street) is denoted by s. It is a homogeneous model in which the heights of buildings are independent and identically distributed (i.i.d.) Rayleigh with parameter γ, that is constant across the entire region. This well-established model has been adopted as part of the International Telecommunication Union Radio Communication Sector (ITU-R) standard [10], [11].

An urban environment is characterized by the following three statistical parameters, 1) α, the ratio of built-up building area to the total area; 2) β, the number of buildings per sq.km; and 3) γ. We note that s and w can be obtained from α, β as follows.

$$w = 1000\sqrt{\frac{\alpha}{\beta}}; \quad s = \frac{1000}{\sqrt{\beta}} - w \tag{1}$$

The parameters α, β and γ for the four urban environments in Table 1 are specified by ITU-R in [11].

For the UAV and UE locations, we consider that the UEs are uniformly distributed in the streets, and the UAV is uniformly likely to be flying over each point on the 2D plane.

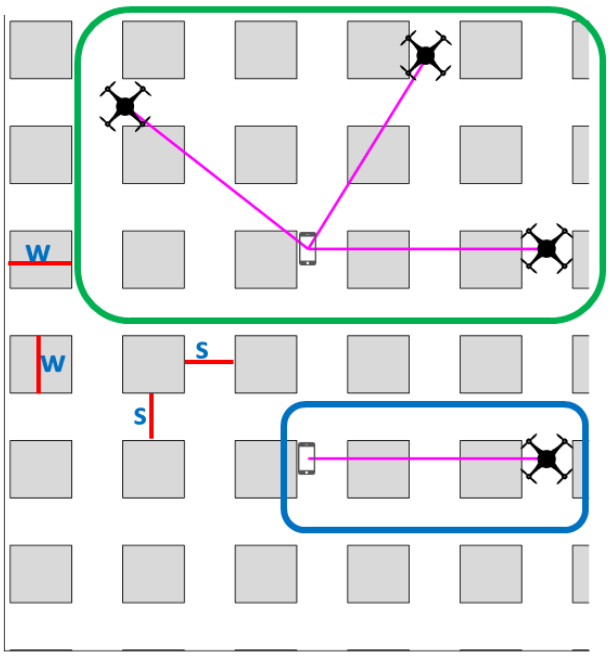

FIGURE 1. A top-down view of the urban environment showing the buildings (grey squares) and streets, as well as example UE and UAV locations. The Blue rectangle illustrates the 1D modelling approach taken in [11]. The Green rectangle illustrates the more accurate 2D modelling approach we take in this paper.

TABLE 1. Parameters for selected environments [11], [12].

Environment	α	β	γ
Suburban	0.1	750	8
Urban	0.3	500	15
Dense Urban	0.5	300	20
High-rise Urban	0.5	300	50

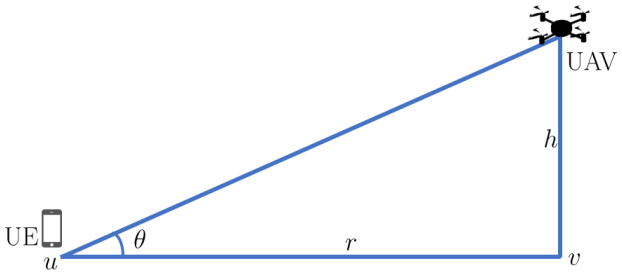

FIGURE 2. Communication link between UAV and UE.

III. PROBLEM FORMULATION

Consider a communication link between a UAV and a ground based UE as shown in Fig. 2. The UAV flies at a height h, above a point v on the ground, that is at a *ground distance* r from the UE at location u, with *elevation angle*, θ.

As mentioned in Section II, we consider that the building heights are i.i.d Rayleigh distributed with parameter γ. Hence, the probability that a building at a ground distance r' from the UE, blocks the direct-path

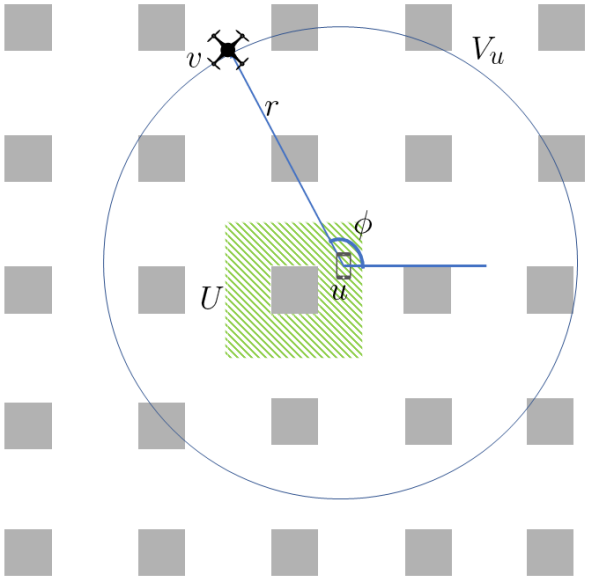

FIGURE 3. Figure depicting the regions U and V_u.

(between UAV and UE) is

$$e^{-\frac{1}{2}\left(\frac{hr'}{\gamma r}\right)^2} \tag{2}$$

For convenience, let $\rho := \frac{h^2}{2\gamma^2 r^2}$.

In order to compute the probability of LoS, we need to formulate a probabilistic model of the UE and UAV locations. Without loss of generality, we will assume that the UEs are uniformly distributed in a square region around a randomly selected building. Let U be the square annulus around the building, i.e., the shaded region in Fig. 3. Consider a UE at location $u \in U$. We will assume that the UAV is uniformly randomly located at a ground distance of r from u, i.e., the distribution of the 2D UAV location is uniformly random on the circle $V_u = \bigcup_{\phi\in(0,2\pi]}\{u + (r\cos(\phi), r\sin(\phi))\}$. Let $\omega := (u, v)$ denote a sample point in $\Omega := \{\omega : u \in U, v \in V_u\}$, which is the set of all possible UE and UAV location pairs.

We define the probability measure μ on Ω in terms of an underlying probability space, which is the set of all (u, ϕ) pairs, where $u \in U$ and $\phi \in (0, 2\pi]$. The ground location of the UAV is a random variable defined by $v(u, \phi) := u + (r\cos(\phi), r\sin(\phi))$. The underlying probability measure μ is the product of the marginals, with u uniformly chosen from U, and ϕ uniformly chosen from $(0, 2\pi]$. The probability measure μ on Ω is then defined by

$$\int_{\omega\in\Omega} f(\omega)\, d\mu(\omega) = \int_{u\in U}\int_{\phi\in[0,2\pi]} f(u, v(u,\phi))\frac{1}{2\pi}\, d\phi\, d\mu_1(u) \tag{3}$$

where f is the indicator of any event of interest, and $\mu_1(\cdot)$ is the uniform probability measure on U. From now on, we will treat Ω as the sample space, with probability measure μ.

A. PROBABILITY OF LoS

Consider an $\omega \in \Omega$. Let $N(\omega)$ be the number of buildings on the line segment between u and v. Let $P_b(\omega, h)$ denote the probability of blockage for a given ω and UAV height h. Let $r_i(\omega)$ be the ground distance between the UE location u (given by ω) and the i^{th} building in the direction of the UAV location v (also given by ω). From (2), we obtain[1]

$$\begin{aligned} P_b(\omega, h) &\triangleq \mathbb{P}(\text{blockage} \mid \omega, h) \\ &= e^{-\rho r_1^2(\omega)} + \sum_{i=2}^{N(\omega)} \Big(\prod_{j=1}^{i-1}(1 - e^{-\rho r_j^2(\omega)})\Big) e^{-\rho r_i^2(\omega)} \end{aligned} \tag{4}$$

The average probability of blockage (i.e., averaged over Ω) for a given UAV height h, and a given ground distance r, is denoted by $P_b(r, h)$, and is given by

$$P_b(r, h) = \int_\Omega P_b(\omega, h) d\mu(\omega) \tag{5}$$

The average probability of LoS, $P_{\text{LoS}}(r, h)$, is given by

$$P_{\text{LoS}}(r, h) = 1 - P_b(r, h) \tag{6}$$

Note that this probability is an average over all possible UAV-UE orientations, whereas the closed-form expression in [36] is for a fixed UAV-BS orientation with respect to the grid (and for a different building and street model, as we discussed in the introduction).

The key idea in this paper is to focus on the role of the first building along the line from the UE to the UAV. For a randomly chosen UE and UAV location pair, i.e., ω is chosen from Ω according to μ, the probability that the direct-path is blocked by the *first* building along the line from the UE to the UAV location, for a given ground distance r, and UAV height h, is denoted by $P_b^1(r, h)$, and is given by

$$P_b^1(r, h) = \int_\Omega e^{-\rho r_1^2(\omega)} d\mu(\omega) \tag{7}$$

The probability that the direct-path is *not* blocked by the first building along the line from the UE to the UAV's location is denoted by $P_{\text{LoS}}^1(r, h)$, which we call the *first-building-LoS probability*, and is given by

$$P_{\text{LoS}}^1(r, h) = 1 - P_b^1(r, h) \tag{8}$$

In the following section, we will provide a lower and upper bound on $P_{\text{LoS}}(r, h)$ in terms of $P_{\text{LoS}}^1(r, h)$.

IV. LOWER AND UPPER BOUNDS ON THE PROBABILITY OF LoS

Let $a_i(\omega, h)$ denote the i-th term in (4) for $i = 1, \ldots, N(\omega)$. This is the probability that the direct-path is blocked by the i^{th} building and not by any of the previous $i - 1$ buildings, for the given (ω, h). We observe that the ratio $\frac{a_{i+1}(\omega,h)}{a_i(\omega,h)}$ is a function of $r_i(\omega)$ and $r_{i+1}(\omega)$, and more particularly, that it is

[1]Note that the full random experiment involves building height realizations for the $N(\omega)$ buildings. We take account of the building heights using (2).

a function of $r_{i+1}(\omega) - r_i(\omega)$ and $r_i(\omega)$. This observation helps us to upper bound the ratio, and will be used later to obtain Theorem 1.

Note that for each $1 \le i \le N(\omega) - 1$,

$$\frac{a_{i+1}(\omega, h)}{a_i(\omega, h)} = \frac{(1 - e^{-\rho r_i^2(\omega)})e^{-\rho r_{i+1}^2(\omega)}}{e^{-\rho r_i^2(\omega)}} \tag{9}$$

Note that from the geometry of the grid, $r_{i+1}(\omega) \ge r_i(\omega) + s$, $\forall\ i$. We use this identity in the RHS of (9), to obtain an upper on the ratio (9) as follows,

$$\begin{aligned}
\frac{a_{i+1}(\omega, h)}{a_i(\omega, h)} &= e^{-\rho(r_{i+1}^2(\omega) - r_i^2(\omega))}(1 - e^{-\rho r_i^2(\omega)}) \\
&\le (e^{-\rho(s^2 + 2r_i(\omega)s)})(1 - e^{-\rho r_i^2(\omega)}) \\
&= e^{-(\frac{\tan^2(\theta)}{2\gamma^2})s^2} e^{-\frac{\tan^2(\theta)}{\gamma^2} r_i(\omega)s} (1 - e^{-(\frac{\tan^2(\theta)}{2\gamma^2}) r_i^2(\omega)}) \\
&\le \max_{\eta \in [0,r]} e^{-\frac{\tan^2(\theta)}{2\gamma^2}s^2} e^{-\frac{\tan^2(\theta)}{\gamma^2}\eta s} (1 - e^{-\frac{\tan^2(\theta)}{2\gamma^2}\eta^2}) \\
&=: c(\theta, r)
\end{aligned} \tag{10}$$

Theorem 1: The probability of Line-of-Sight, $P_{LoS}(r, h)$, is bounded above and below, as follows

$$\frac{P_{LoS}^1(r, h) - c(\theta, r)}{1 - c(\theta, r)} \le P_{LoS}(r, h) \le P_{LoS}^1(r, h) \tag{11}$$

Proof: Using (10), we obtain the upper bound on the ratio $\frac{a_{i+1}(\omega,h)}{a_1(\omega,h)}$ as follows,

$$\begin{aligned}
\frac{a_{i+1}(\omega, h)}{a_1(\omega, h)} &= \frac{a_{i+1}(\omega, h)}{a_i(\omega, h)} \times \frac{a_i(\omega, h)}{a_{i-1}(\omega, h)} \times \ldots \times \frac{a_2(\omega, h)}{a_1(\omega, h)} \\
&\le c^i(\theta, r)
\end{aligned} \tag{12}$$

From (4), (10) and (12), we obtain

$$a_1(\omega, h) \le P_b(\omega, h) \le \sum_{i=1}^{N(\omega)} a_1(\omega, h) c^{i-1}(\theta, r) \tag{13}$$

$$a_1(\omega, h) \le P_b(\omega, h) \le a_1(\omega, h) \frac{1}{1 - c(\theta, r)} \tag{14}$$

By integrating (14) over Ω, we obtain

$$\begin{aligned}
\int_\Omega a_1(\omega, h) d\mu(\omega) &\le \int_\Omega P_b(\omega, h) d\mu(\omega) \\
&\le \int_\Omega \frac{a_1(\omega, h)}{1 - c(\theta, r)} d\mu(\omega) \\
P_b^1(r, h) \le P_b(r, h) &\le \frac{P_b^1(r, h)}{1 - c(\theta, r)}
\end{aligned} \tag{15}$$

The theorem is now immediate from (8). ∎

Fig. 4 shows $\frac{P_{\text{LoS}}^1(r,h) - c(\theta,r)}{1 - c(\theta,r)}$, $P_{\text{LoS}}(r, h)$, and $P_{\text{LoS}}^1(r, h)$ curves for different urban environments for UAV height $h = 500$m. From the figure, it can be observed that the gap between the lower-bound $\frac{P_{\text{LoS}}^1(r,h) - c(\theta,r)}{1 - c(\theta,r)}$ and $P_{\text{LoS}}(r, h)$ increases with the ground distance. The upper-bound $P_{\text{LoS}}^1(r, h)$ is very close to the $P_{\text{LoS}}(r, h)$ curve,

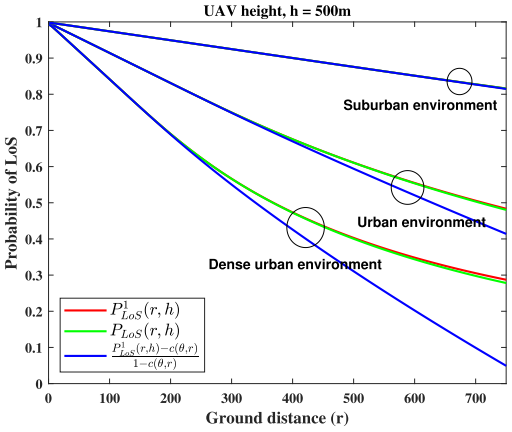

FIGURE 4. $\frac{P_{\text{LoS}}^1(r,h) - c(\theta,r)}{1 - c(\theta,r)}$, $P_{\text{LoS}}(r, h)$, and $P_{\text{LoS}}^1(r, h)$ curves for different urban environments for UAV height, $h = 500$m.

although as the ground distance increases, for a given height (or in other words the elevation angle, θ decreases), the gap increases slightly. This is because the impact of the 2nd, 3rd, 4th, ... buildings along the line between the UE and the UAV ground location are greater at lower elevation angles. Even so, the gap remains small.

In fact, we have found that the upper bound is close for all the UAV heights and ground distances we have investigated. Therefore we suggest that the first-building-LoS probability $P_{\text{LoS}}^1(r, h)$ can be used as an excellent estimate of $P_{\text{LoS}}(r, h)$.

V. STATISTICAL MODELING OF THE FIRST BUILDING DISTANCE

In this section, we statistically model the distance to the first building for a UE-UAV location pair, ω, that is randomly selected (over Ω according to the probability measure μ). This distance is a random variable, r_1, that we call the *first-building-distance*. Its probability density function (PDF), $p_{r_1}(x)$, $x \ge 0$, is defined by

$$\begin{aligned}
p_{r_1}(x) &:= \frac{d}{dx} \mathbb{P}[r_1 \le x] \\
&= \frac{d}{dx} \int_{\omega \in \Omega} \mathbf{1}[r_1(\omega) \le x]\, d\mu(\omega)
\end{aligned}$$

where $\mathbf{1}[\cdot]$ is the indicator function, and $r_1(\omega)$ is a realization of r_1 for a specific UE-UAV pair defined by ω.

The first-building-LoS probability can be written in terms of the PDF $p_{r_1}(x)$ using (8), as follows

$$P_{\text{LoS}}^1(r, h) = 1 - \int_0^r p_{r_1}(x) e^{-\rho x^2} dx \tag{16}$$

We now model $p_{r_1}(\cdot)$ using empirical simulations for various street parameter values, (s, w). We use a family of parametric density functions to model the empirical probability density function (PDF). We then provide values of the parameters as functions of (s, w). We use the parametric density functions to compute $P_{\text{LoS}}^1(r, h)$ ($\approx P_{\text{LoS}}(r, h)$), and provide closed form expressions. Our formulas can be applied

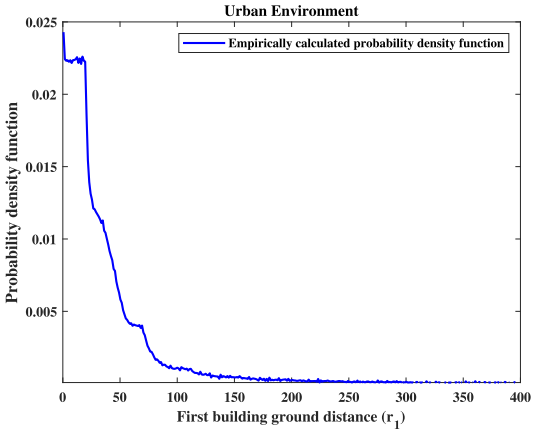

FIGURE 5. Empirically calculated PDF of distance to the first building along the LoS.

to any of the four urban environments in Table 1, and more generally to any grid geometry-based urban environment.

Fig. 5 shows an empirical estimate of $p_{r_1}(\cdot)$, which we denote $\hat{p}_{r_1}(\cdot)$, derived in this case from simulations of the Urban environment (see Table 1). The curve shows nonlinear features that are a function of the square nature of the geometric street grid model and the parameters s and w. In the following, we use empirical estimates to derive two mathematical models to approximate $p_{r_1}(\cdot)$.

A. EXPONENTIAL MODELING OF PDF

We have observed in general, for a range of grid geometry-based urban environments (with different s and w values), that in each case the empirical PDF, $\hat{p}_{r_1}(\cdot)$, has a shape similar to that in Fig. 5. This observation leads us to consider modelling $\hat{p}_{r_1}(\cdot)$ with an exponential PDF as follows

$$f_{r_1}(x) = \lambda_1 e^{-\lambda_1 x}, \ \forall\, x \geq 0 \tag{17}$$

where we propose to calculate the parameter λ_1, for a given (s, w) pair, from $\hat{p}_{r_1}(\cdot)$ using a least squares approach, as follows

$$\lambda_1 = \arg\min_{\lambda} \sum_{x=0}^{L} \left(\lambda e^{-\lambda x} - \hat{p}_{r_1}(x)\right)^2. \tag{18}$$

The summation in (18) is over integer values of distance in metres. Fig. 5 shows that the probability density has dropped to essentially zero by about 250 m. We choose the upper limit $L = 2500$ m in our numerical results to ensure that the exponential approximation function will also be essentially zero for correspondingly large distances.

We now present a key observation that allows us to generalise the exponential model by providing an alternate expression for λ_1, in terms of s and w. We note that for a fixed value of the ratio $\frac{s}{w}$, the geometric street grid scales linearly with the value of s. This important scaling property observation helps to relate the PDF of r_1 between grids of different dimensions. Suppose $p_{r_1}(x)$ is known for a grid with dimensions (s, w), then the PDF for a grid with dimensions (ks, kw) is given by $\frac{1}{k} p_{r_1}(x/k)$.

Therefore, if $\lambda_1 = \lambda'$ is the parameter for a grid with dimensions (s_1, w_1), then the parameter for a grid with dimensions (ks_1, kw_1) is $\lambda_1 = \frac{\lambda'}{k}$. Thus, the quantity $s\lambda_1$ is invariant for all grids with a fixed value of $\frac{s}{w}$. Hence, we conclude that $s\lambda_1$ only depends on the ratio $\frac{s}{w}$.

We have computed the quantity $s\lambda_1$ for various grid configurations (i.e., various (s, w)), with $\frac{s}{w}$ values ranging from 0.25 to 2.5 (note that all four urban environments have an $\frac{s}{w}$ value in this range). We then used a polynomial fit to provide the following estimate for λ_1 as follows

$$\hat{\lambda}_1 = \frac{1}{s}\left(\frac{613}{753} - \frac{901}{2116}\left(\frac{s}{w}\right) + \frac{1258}{8477}\left(\frac{s}{w}\right)^2 - \frac{239}{10712}\left(\frac{s}{w}\right)^3\right) \tag{19}$$

We see in Section VIII that this expression provides accurate results for a wide range of (s, w).

B. PIECE-WISE MODELING OF PDF

In this section we introduce a more sophisticated model, that captures the piece-wise nature of $\hat{p}_{r_1}(\cdot)$. In particular, we note that there is an even distribution of small first-building-distance values, since the streets are straight and we are assuming a uniform distribution of UEs in the streets. Over many values of (s, w), we have observed that the PDF $\hat{p}_{r_1}(\cdot)$ tends to be mostly flat from 0 to s, and has an approximately exponential trend after s. This observation leads us to consider modelling $\hat{p}_{r_1}(\cdot)$ as follows,

$$g_{r_1}(x) = \begin{cases} A_2/s & x \leq s, \\ (1 - A_2)\lambda_2 e^{-\lambda_2(x-s)} & x > s, \end{cases} \tag{20}$$

where we propose to calculate the parameters A_2 and λ_2, for a given (s, w) pair, from $\hat{p}_{r_1}(\cdot)$ using a least squares approach, as follows

$$A_2 = \arg\min_{A} \sum_{x=0}^{\lfloor s \rfloor} (A/s - \hat{p}_{r_1}(x))^2 \tag{21}$$

$$\lambda_2 = \arg\min_{\lambda} \sum_{x=\lceil s \rceil}^{2500} \left((1 - A_2)\lambda e^{-\lambda(x-s)} - \hat{p}_{r_1}(x)\right)^2 \tag{22}$$

We have computed the parameter A_2 and λ_2 for various grid configurations (i.e., various (s, w)), with $\frac{s}{w}$ values ranging from 0.25 to 2.5 (note that all four urban environments have an $\frac{s}{w}$ value in this range). As with the exponential modelling, we then used a polynomial fit to provide the following estimate for A_2 and λ_2 as follows

$$\hat{A}_2 = \left(\frac{634}{403} + \frac{457}{601}\left(\frac{s}{w}\right)\right)^{-1} \tag{23}$$

$$\hat{\lambda}_2 = \frac{1}{s}\left(\frac{827}{951} - \frac{139}{341}\left(\frac{s}{w}\right) + \frac{420}{3113}\left(\frac{s}{w}\right)^2 - \frac{127}{6176}\left(\frac{s}{w}\right)^3\right) \tag{24}$$

We see in Section VIII that this expression provides accurate results for a wide range of (s, w). When compared

to our exponential model (17), we will see that this model is more accurate. In some applications, however, (17) may be more desirable since it does not involve discontinuities and is therefore more amenable for optimization.

VI. PROBABILITY OF LoS ESTIMATION USING PARAMETERIZED MODELS

As mentioned in Section V, the first-building-LoS probability, $P^1_{\text{LoS}}(r,h)$, can be calculated using (16). In this section, we replace $p_{r_1}(\cdot)$ in (16), with each of our proposed models $f_{r_1}(\cdot)$ from (17), and $g_{r_1}(\cdot)$ from (20), to give the following propositions, which provide closed-form expressions for the average probability of line-of-sight.

Proposition 1: For an urban environment with parameters α, β and γ, the LoS probability $P_{LoS}(r,h)$ is accurately estimated, using (17) and (19), by

$$\begin{aligned}
&\hat{P}^1_{LoS}(r,h)\\
&= 1-\int_0^r f_{r_1}(x)e^{-\rho x^2}dx\\
&\approx 1-\int_0^r \hat{\lambda}_1 e^{-\hat{\lambda}_1 x}e^{-\rho x^2}dx \quad \textit{using (19)}\\
&= 1-\hat{\lambda}_1\frac{\sqrt{\pi}e^{\frac{\hat{\lambda}_1^2}{4\rho}}}{2\sqrt{\rho}}\left(erf\Big(\frac{2\rho r+\hat{\lambda}_1}{2\sqrt{\rho}}\Big)-erf\Big(\frac{\hat{\lambda}_1}{2\sqrt{\rho}}\Big)\right)\\
&=: F(r,h|\alpha,\beta,\gamma) \qquad (25)
\end{aligned}$$

where $erf(\cdot)$ is the error function, and $\rho=\frac{h^2}{2\gamma^2 r^2}$.

Proposition 2: For an urban environment with parameters α, β and γ, the LoS probability $P_{LoS}(r,h)$ is accurately estimated, using (20), (23) and (24), by

$$\begin{aligned}
&\tilde{P}^1_{LoS}(r,h)\\
&= 1-\int_0^r g_{r_1}(x)e^{-\rho x^2}dx\\
&\approx \begin{cases} 1-\int_0^r \frac{\hat{A}_2}{s}e^{-\rho x^2}dx & r\le s,\\ 1-\int_0^s \frac{\hat{A}_2}{s}e^{-\rho x^2}dx & \\ \quad -\int_s^r (1-\hat{A}_2)\hat{\lambda}_2 e^{-\hat{\lambda}_2(x-s)}e^{-\rho x^2}dx & r>s, \end{cases}\\
&= \begin{cases} 1-\sqrt{\pi}\frac{\hat{A}_2}{s}\frac{erf(\sqrt{\rho}r)}{2\sqrt{\rho}} & r\le s,\\ 1-\sqrt{\pi}\frac{\hat{A}_2}{s}\frac{erf(\sqrt{\rho}s)}{2\sqrt{\rho}}-(1-\hat{A}_2)\hat{\lambda}_2 e^{\hat{\lambda}_2 s}* & \\ \quad \frac{\sqrt{\pi}e^{\frac{\hat{\lambda}_2^2}{4\rho}}(erf(\frac{2\rho r+\hat{\lambda}_2}{2\sqrt{\rho}})-(erf(\frac{2\rho s+\hat{\lambda}_2}{2\sqrt{\rho}}))}{2\sqrt{\rho}} & r>s \end{cases}\\
&=: G(r,h|\alpha,\beta,\gamma) \qquad (26)
\end{aligned}$$

where $erf(\cdot)$ is the error function, and $\rho=\frac{h^2}{2\gamma^2 r^2}$.

As mentioned earlier, our model $g_{r_1}(\cdot)$ in (20), is a more accurate representation of $\hat{p}_{r_1}(\cdot)$ compared to $f_{r_1}(\cdot)$ in (17). Therefore, $G(r,h|\alpha,\beta,\gamma)$ is a more accurate estimate of the first-building-LoS probability compared to $F(r,h|\alpha,\beta,\gamma)$. However, following the same argument as previously, it may be more desirable to employ $F(r,h|\alpha,\beta,\gamma)$ in some applications, since it does not involve discontinuities and is therefore more amenable for optimization.

In the Section VIII, we will show that both estimates are in close agreement with the actual probability of LoS using Monte-Carlo simulation.

VII. AREA LoS PROBABILITY

An important application of our results is to a cellular system in which the UAV is an aerial base station. A coverage metric of interest is the proportion of the cell around the UAV that has LoS connectivity, when the UAV is at a height h above the ground. We model the cell as a circular region of radius R around the point on the ground directly below the UAV.

We define the *Area LoS probability* $P_{ALoS}(R,h)$ as the probability that a LoS link exists between a UAV and a UE located uniformly *within* a circle of radius R. An equivalent definition of Area LoS probability was considered in [36] where the UAV was uniformly located within a circular region around the fixed ground BS. However, the expression given in [36] erroneously takes the distance between the UAV and ground BS to be a uniform random variable. We provide the expression for the case in which the UE is uniformly distributed in the circular region below.

$$P_{ALoS}(R,h)=\int_0^R \frac{2r}{R^2}P_{LoS}(r,h)dr \qquad (27)$$

We provide an efficient approach to evaluate the area LoS probability $P_{ALoS}(R,h)$ in the following. Firstly, we obtain (28) using integration by parts. We have observed that the slope of the LoS function $\frac{\partial P_{LoS}(r,h)}{\partial r}$ changes slowly w.r.t r (See Fig. 6-Fig. 10 in Section VIII). Hence, $P_{ALoS}(R,h)$ can be efficiently approximated using numerical integration (i.e., reasonable values of N) as in (29).

$$\begin{aligned}
&P_{ALoS}(R,h)\\
&= P_{LoS}(R,h)-\int_0^R \frac{r^2}{R^2}\frac{\partial P_{LoS}(r,h)}{\partial r}dr \qquad (28)\\
&\approx P_{LoS}(R,h)-\sum_{i=1}^{N}\int_{r_{i-1}}^{r_i}\frac{r^2}{R^2}\frac{P_{LoS}(r_i,h)-P_{LoS}(r_{i-1},h)}{\Delta}dr \qquad (29)\\
&= P_{LoS}(R,h)-\sum_{i=1}^{N}\frac{r_i^3-r_{i-1}^3}{3R^2}\frac{P_{LoS}(r_i,h)-P_{LoS}(r_{i-1},h)}{\Delta} \qquad (30)
\end{aligned}$$

where N is the number of steps in the numerical integration, $\Delta:=\frac{R}{N}$ and $r_i:=i\Delta$.

We now obtain the expressions for area LoS probability $P_{ALoS}(r,h)$ by applying our first building LoS approximations. As such, (31) is obtained using Proposition 1 and (32)

is obtained using Proposition 2.

$$P_{ALoS}(R,h) \approx F(R,h|\alpha,\beta,\gamma) - \sum_{i=1}^{N} \frac{r_i^3 - r_{i-1}^3}{3R^2} \frac{F_i - F_{i-1}}{\Delta} \tag{31}$$

$$P_{ALoS}(R,h) \approx G(R,h|\alpha,\beta,\gamma) - \sum_{i=1}^{N} \frac{r_i^3 - r_{i-1}^3}{3R^2} \frac{G_i - G_{i-1}}{\Delta} \tag{32}$$

where $F_i = F(r_i, h|\alpha,\beta,\gamma)$ and $G_i = G(r_i, h|\alpha,\beta,\gamma)$.

VIII. NUMERICAL RESULTS

In this section, we compare our proposed methods in Propositions 1 and 2, with existing approaches, and results from the Monte-Carlo simulation. Our methods, and the existing approaches we compare with, all assume a homogeneous built environment as described in Section II in which the building heights are independently and randomly drawn from the same Rayleigh distribution. We provide numerical results for the homogeneous built environment, including both average and area LoS probabilities, in Sections VIII-A. In Section VIII-B, we explore the application of our results to inhomogeneous scenarios.

A. HOMOGENEOUS BUILT ENVIRONMENTS

Fig. 6 shows the average probability of LoS curves for the Urban environment, as a function of ground distance, for two different UAV heights. The (dash-dot) red curve is the estimated probability of LoS using the expression given in [11]. This curve is a staircase because of the 'floor' function used in [11]. The (dash-dot) blue curve is the estimated probability of LoS using the expression given in [14]. Our proposed estimates $F(r,h|\alpha,\beta,\gamma)$ (solid magenta) and $G(r,h|\alpha,\beta,\gamma)$ (solid green) are also plotted, in addition to the Monte-Carlo curves which were generated by randomly generating building heights and randomly locating a UE on a street. The UAV was randomly located in the plane at height h above the streets, and only above the buildings which are lower than height h (i.e., not inside buildings that are taller than h). Ray tracing was done to establish whether there is LoS, and then this process was repeated many times. The figure shows that our proposed probability of LoS using the two proposed PDFs is in close agreement with the Monte-Carlo simulation.

Figs. 7, 8 and 9 show the probability of LoS for other urban environments. From the figures, we can see that the proposed probability of LoS aligns very well with the Monte-Carlo simulation in each case.

As mentioned earlier, our proposed method can also be applied to other environments, i.e., not restricted to just four urban environments. Many urban regions have a mixture of building types and street configurations. For example, for area containing a mixture of mid-rise shopping centre buildings with surrounding houses, the parameters could be $\alpha = 0.25$, $\beta = 400$, and $\gamma = 10$. Fig. 10 shows the probability of LoS curves for this environment. The figure shows our proposed probability of LoS aligns very well with the Monte-Carlo simulation.

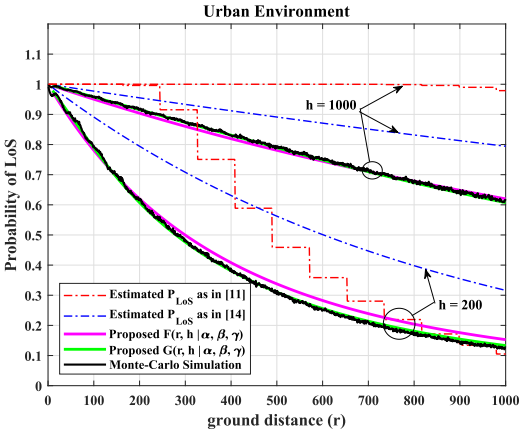

FIGURE 6. Probability of line-of-sight for a fixed height and various ground distances for urban environment. Here, UAV height h and ground distance r are in meters.

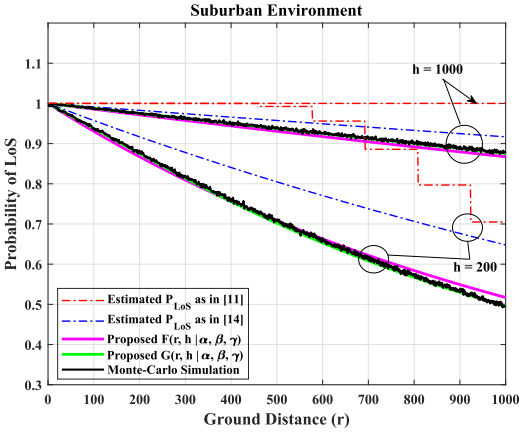

FIGURE 7. Probability of line-of-sight for a fixed height and various ground distances for suburban environment. Here, UAV height h and ground distance r are in meters.

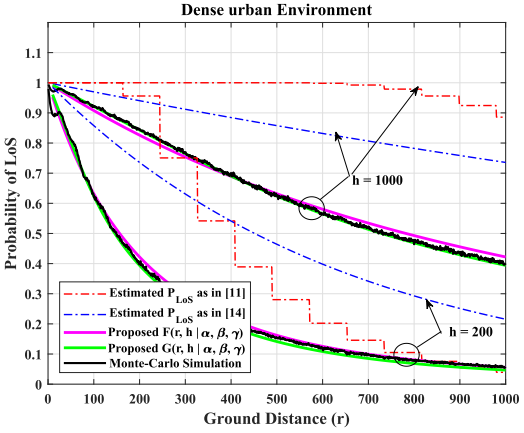

FIGURE 8. Probability of line-of-sight for a fixed height and various ground distances for dense urban environment. Here, UAV height h and ground distance r are in meters.

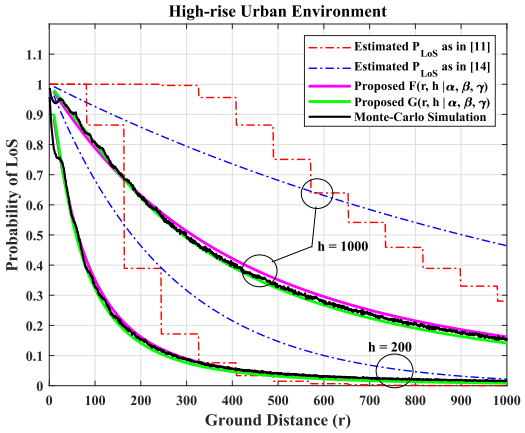

FIGURE 9. Probability of line-of-sight for a fixed height and various ground distances for high-rise urban environment. Here, UAV height h and ground distance r are in meters.

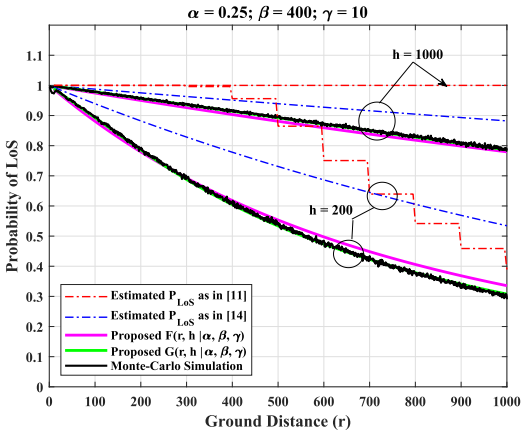

FIGURE 10. Probability of line-of-sight for a fixed height and various ground distances for an environment with $\alpha = 0.25$, $\beta = 400$, and $\gamma = 10$. Here, UAV height h and ground distance r are in meters.

Figs. 11-13 show the Area LoS probability curves for UAV heights $h = 200$m and 1000 m, for various built environments. In each figure, the Monte-Carlo curve is obtained from (27), where $P_{LoS}(r, h)$ is obtained by Monte-Carlo Simulation. It can be observed that our expressions (31) and (32) provide highly accurate Area LoS probabilities even for small N.

B. IN-HOMOGENEOUS BUILT ENVIRONMENTS

In a practical setting, the coverage area of a UAV can be large enough in some scenarios to cover multiple urban environments. For example, consider a UAV flying in the central part of a city with high-rise buildings, and communicating with UEs in a nearby suburban area. The buildings between the UAV and UE are a mixture of suburban and high-rise buildings, which have different Rayleigh parameters.

Our key observation from the homogeneous case is that the LoS probability is mainly determined by the buildings closest to the UE. In the in-homogeneous scenario we propose

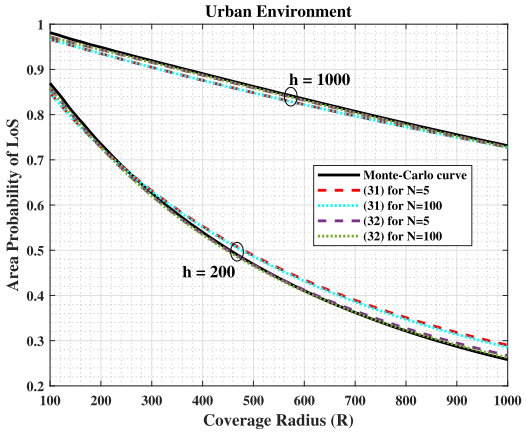

FIGURE 11. Area LoS probability for UAV height h and coverage radius R in urban environment. Here, R and h are in meters.

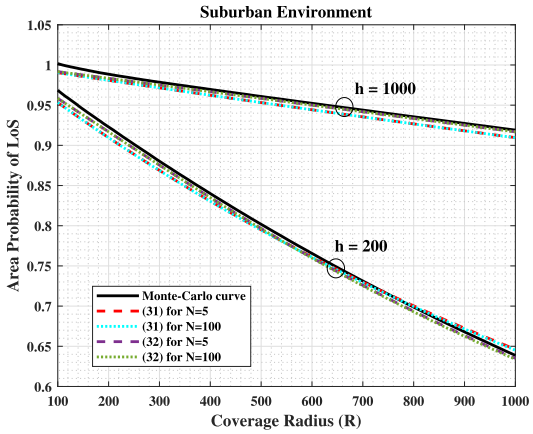

FIGURE 12. Area LoS probability for UAV height h and coverage radius R in suburban environment. Here, R and h are in meters.

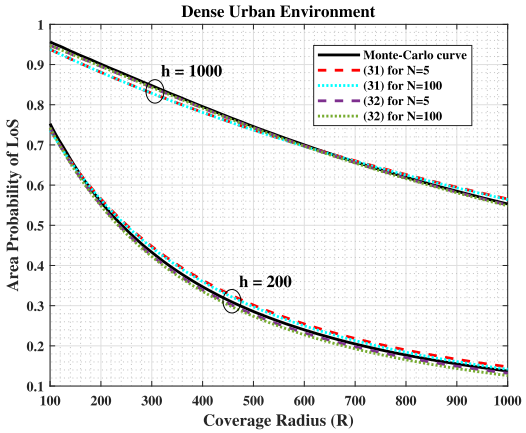

FIGURE 13. Area LoS probability for UAV height h and coverage radius R in dense urban environment. Here, R and h are in meters.

to use this as a method to predict the LoS probability more generally, based on the building heights in a local region around the UE. We define a square inner region of dimension $8s + 9w$, in which the UE's location is uniformly distributed around the building that is at the centre of the square,

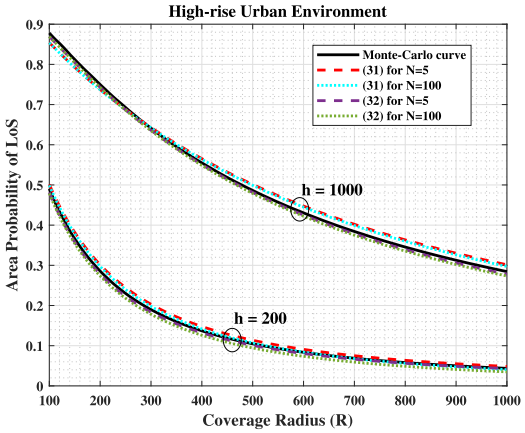

FIGURE 14. Area LoS probability for UAV height *h* and coverage radius *R* in high-rise urban environment.Here, *R* and *h* are in meters.

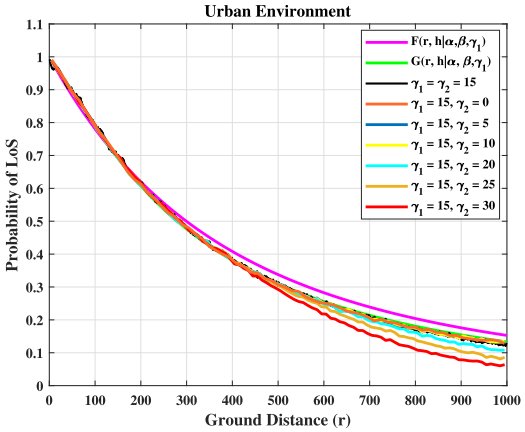

FIGURE 15. Figure showing results with the inner region as the urban environment and outer region with different Rayleigh parameters γ_2. The curves are obtained from Monte-Carlo simulation results. The results are shown for UAV height 200m.

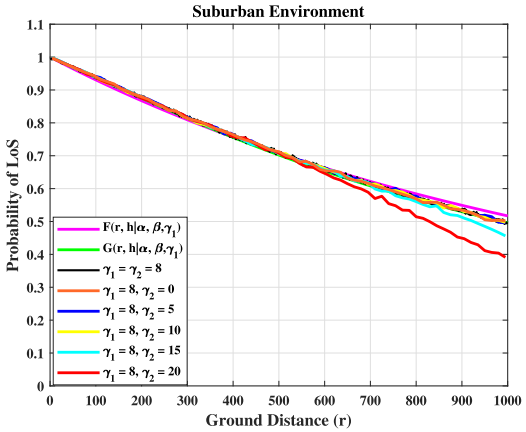

FIGURE 16. Figure showing results with the inner region as the suburban environment and outer region with different Rayleigh parameters γ_2. The curves are obtained from Monte-Carlo simulation results. The results are shown for UAV height 200m.

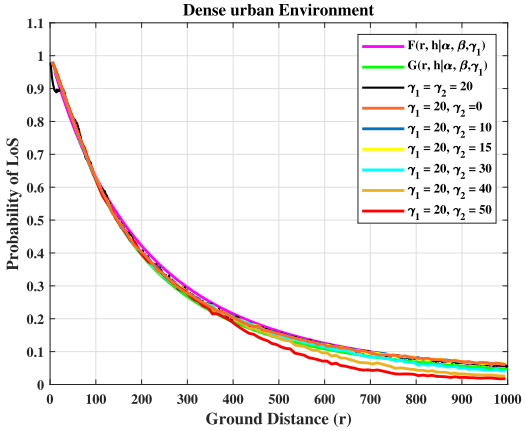

FIGURE 17. Figure showing results with the inner region as the dense urban environment and outer region with different Rayleigh parameters γ_2. The curves are obtained from Monte-Carlo simulation results. The results are shown for UAV height 200m.

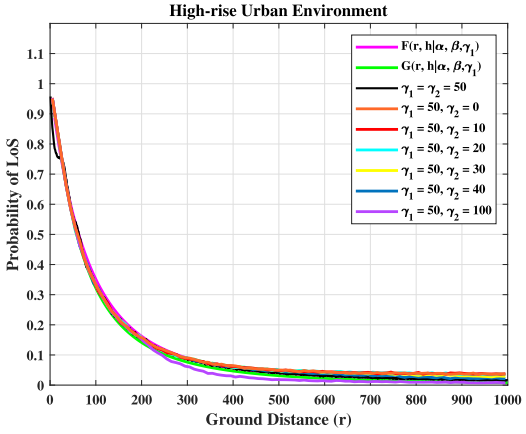

FIGURE 18. Figure showing results with the inner region as the high-rise urban environment and outer region with different Rayleigh parameters γ_2. The curves are obtained from Monte-Carlo simulation results. The results are shown for UAV height 200m.

as illustrated in Fig. 3. This square thus contains 4 buildings in each rectangular direction from the UE. All the buildings in the inner region have heights that are *i.i.d.* with Rayleigh parameter γ_1. We consider in-homogeneous scenarios where all the buildings outside the inner region have heights that are *i.i.d.* with Rayleigh parameter γ_2.

Since the first buildings are highly likely to be in the inner region, we hypothesize that the first-building-LoS-probability derived using the inner region parameters will accurately determine the LoS probability in this in-homogeneous case, provided the difference between γ_2 and γ_1 is not too large. Using Monte-Carlo simulations, in Fig. 15-Fig. 18, we provide the acceptable range for γ_2 and elevation angles, considering each of the four urban environments for the inner region.

Fig. 15 shows results when the inner region is an urban environment (from Table. 1), and the UAV height is 200m. The figure shows that our proposed first-building-LoS probability models are accurate for outer region Rayleigh parameter values of $\gamma_2 \leq \gamma_1$ over the full range of ground distances. For values of γ_2 in the range $\gamma_1 < \gamma_2 \leq 2\gamma_1$, our model is accurate for ground distances less than 400m. Note

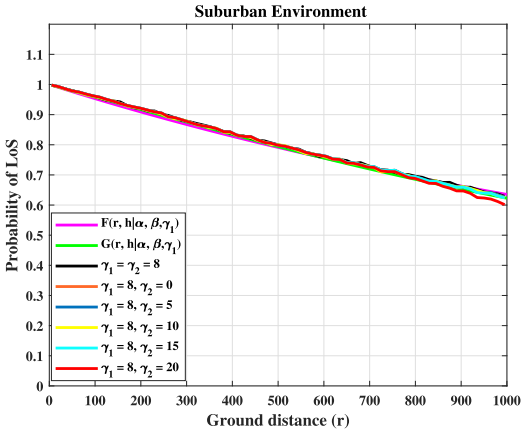

FIGURE 19. Figure showing results with the inner region as the suburban environment and outer region with different Rayleigh parameters γ_2. The curves are obtained from Monte-Carlo simulation results. The results are shown for UAV height 300m.

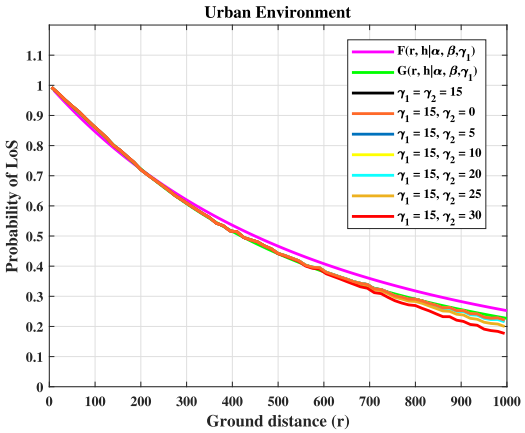

FIGURE 20. Figure showing results with the inner region as the urban environment and outer region with different Rayleigh parameters γ_2. The curves are obtained from Monte-Carlo simulation results. The results are shown for UAV height 300m.

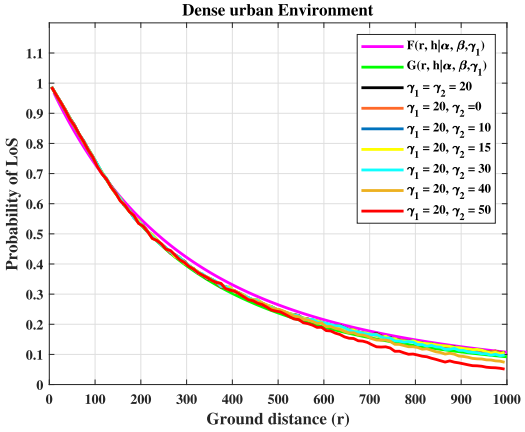

FIGURE 21. Figure showing results with the inner region as the dense urban environment and outer region with different Rayleigh parameters γ_2. The curves are obtained from Monte-Carlo simulation results. The results are shown for UAV height 300m.

that the ground distance of 400m corresponds to an elevation angle of $\approx$ 25°, so our results hold for all elevation angles greater than 25°.

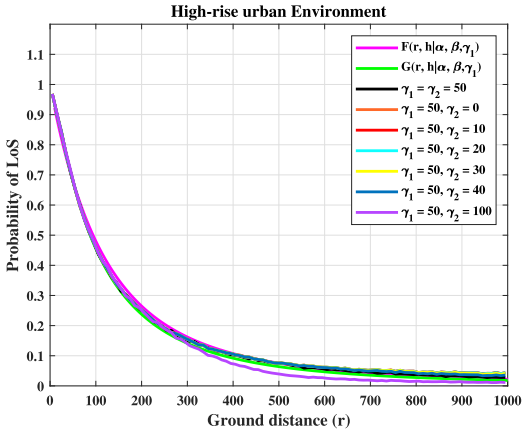

FIGURE 22. Figure showing results with the inner region as the high-rise urban environment and outer region with different Rayleigh parameters γ_2. The curves are obtained from Monte-Carlo simulation results. The results are shown for UAV height 300m.

Fig. 16, Fig. 17 and Fig. 18 show results for the case when the inner region is suburban, dense urban, and high-rise urban respectively. From the figures, we can see that our proposed first-building-LoS probability models are accurate for the same range of parameter values as in Fig. 15.

For a range of other UAV heights, we have observed that the same results hold. For example, Fig. 19, 20, 21, and 22 show results for the case when the inner region is suburban, urban, dense urban, and high-rise urban respectively for the UAV height of 300m. From the figures, we can see that our proposed first-building-LoS probability models are accurate for outer region Rayleigh parameter values of $\gamma_2 \leq \gamma_1$ over the full range of ground distances. For values of γ_2 in the range $\gamma_1 < \gamma_2 \leq 2\gamma_1$, our model is accurate for ground distances less than 650m. Note that the ground distance of 650m corresponds to an elevation angle of $\approx$ 25°, so our results hold for all elevation angles greater than 25°.

IX. CONCLUSION

We presented a new approach to estimate the probability of LoS for UAV communications in urban environments where the building heights are modeled by a homogeneous Rayleigh distribution.

We have provided a lower and upper bound on the average probability of LoS, which are given in terms of the first-building-LoS probability. We provided two statistical models for first-building-distance. We then developed a novel method for calculating the first-building-LoS probability, and presented two general closed-form estimates of the first-building-LoS probability. We showed that this approach provides very good estimates for the average probability of LoS, and that our closed-form formulas are significantly more accurate than existing approaches. We expect that our first-building approach to line-of-sight calculations can be applied to more general settings, with different city block models and building distributions.

We have also provided a new approach to estimate the Area Probability of LoS. Using our estimates for first-building-LoS probability, we provided two accurate closed-form estimates for the Area Probability of LoS.

We also explored the application of our results to inhomogeneous scenarios in which an outer region can have a different building height parameter than an inner region closer to the UE. In these scenarios, we have found our formulas are still accurate provided that the outer region building height parameter is no more than twice that of the inner region close to the UE, and the angle of elevation to the UAV is at least 25 degrees. Future work can consider further extensions to more general inhomogeneous scenarios.

REFERENCES

[1] S. Sekander, H. Tabassum, and E. Hossain, "Multi-tier drone architecture for 5G/B5G cellular networks: Challenges, trends, and prospects," *IEEE Commun. Mag.*, vol. 56, no. 3, pp. 96–103, Mar. 2018.

[2] M. Mozaffari, W. Saad, M. Bennis, and M. Debbah, "Drone small cells in the clouds: Design, deployment and performance analysis," in *Proc. IEEE Global Commun. Conf. (GLOBECOM)*, Dec. 2015, pp. 1–6.

[3] M. Mozaffari, W. Saad, M. Bennis, Y.-H. Nam, and M. Debbah, "A tutorial on UAVs for wireless networks: Applications, challenges, and open problems," *IEEE Commun. Surveys Tuts.*, vol. 21, no. 3, pp. 2334–2360, 3rd Quart., 2019.

[4] I. Bucaille, S. Héthuin, A. Munari, R. Hermenier, T. Rasheed, and S. Allsopp, "Rapidly deployable network for tactical applications: Aerial base station with opportunistic links for unattended and temporary events ABSOLUTE example," in *Proc. IEEE Mil. Commun. Conf. (MILCOM)*, Nov. 2013, pp. 1116–1120.

[5] P. Zhan, K. Yu, and A. L. Swindlehurst, "Wireless relay communications with unmanned aerial vehicles: Performance and optimization," *IEEE Trans. Aerosp. Electron. Syst.*, vol. 47, no. 3, pp. 2068–2085, Jul. 2011.

[6] M. Mozaffari, W. Saad, M. Bennis, and M. Debbah, "Efficient deployment of multiple unmanned aerial vehicles for optimal wireless coverage," *IEEE Commun. Lett.*, vol. 20, no. 8, pp. 1647–1650, Aug. 2016.

[7] I. Bekmezci, O. K. Sahingoz, and Ş. Temel, "Flying ad-hoc networks (FANETs): A survey," *Ad Hoc Netw.*, vol. 11, no. 3, pp. 1254–1270, 2013.

[8] A. Al-Hourani, S. Kandeepan, and S. Lardner, "Optimal LAP altitude for maximum coverage," *IEEE Wireless Commun. Lett.*, vol. 3, no. 6, pp. 569–572, Dec. 2014.

[9] M. Alzenad, A. El-Keyi, F. Lagum, and H. Yanikomeroglu, "3-D placement of an unmanned aerial vehicle base station (UAV-BS) for energy-efficient maximal coverage," *IEEE Wireless Commun. Lett.*, vol. 6, no. 4, pp. 434–437, Aug. 2017.

[10] *Propagation Data and Prediction Methods Required for the Design of Terrestrial Broadband Radio Access Systems Operating in a Frequency Range From 3 to 60 GHz*, document ITU-R P.1410-5, 1999.

[11] *Propagation Data and Prediction Methods Required for the Design of Terrestrial Broadband Radio Access Systems Operating in a Frequency Range From 3 to 60 GHz*, document ITU-R P.1410-5, 2013.

[12] J. Holis and P. Pechac, "Elevation dependent shadowing model for mobile communications via high altitude platforms in built-up areas," *IEEE Trans. Antennas Propag.*, vol. 56, no. 4, pp. 1078–1084, Apr. 2008.

[13] I. Atzeni, J. Arnau, and M. Kountouris, "Downlink cellular network analysis with LOS/NLOS propagation and elevated base stations," *IEEE Trans. Wireless Commun.*, vol. 17, no. 1, pp. 142–156, Jan. 2017.

[14] H. Kang, J. Joung, J. Ahn, and J. Kang, "Secrecy-aware altitude optimization for quasi-static UAV base station without eavesdropper location information," *IEEE Commun. Lett.*, vol. 23, no. 5, pp. 851–854, May 2019.

[15] Z. Yang, L. Zhou, G. Zhao, and S. Zhou, "Blockage modeling for inter-layer UAVs communications in urban environments," in *Proc. 25th Int. Conf. Telecommun. (ICT)*, Jun. 2018, pp. 307–311.

[16] Q. Feng, E. K. Tameh, A. R. Nix, and J. McGeehan, "WLCp2–06: Modelling the likelihood of line-of-sight for air-to-ground radio propagation in urban environments," in *Proc. IEEE Globecom*, Nov. 2006, pp. 1–5.

[17] R. I. Bor-Yaliniz, A. El-Keyi, and H. Yanikomeroglu, "Efficient 3-D placement of an aerial base station in next generation cellular networks," in *Proc. IEEE Int. Conf. Commun. (ICC)*, May 2016, pp. 1–5.

[18] E. Kalantari, H. Yanikomeroglu, and A. Yongacoglu, "On the number and 3D placement of drone base stations in wireless cellular networks," in *Proc. IEEE 84th Veh. Technol. Conf. (VTC-Fall)*, Sep. 2016, pp. 1–6.

[19] Y. Chen, N. Li, C. Wang, W. Xie, and J. Xv, "A 3D placement of unmanned aerial vehicle base station based on multi-population genetic algorithm for maximizing users with different QoS requirements," in *Proc. IEEE 18th Int. Conf. Commun. Technol. (ICCT)*, Oct. 2018, pp. 967–972.

[20] N. Adam, C. Tapparello, W. Heinzelman, and H. Yanikomeroglu, "Placement optimization of multiple UAV base stations," in *Proc. IEEE Wireless Commun. Netw. Conf. (WCNC)*, Apr./May 2021, pp. 1–7.

[21] X. Zhong, Y. Huo, X. Dong, and Z. Liang, "QoS-compliant 3-D deployment optimization strategy for UAV base stations," *IEEE Syst. J.*, vol. 15, no. 2, pp. 1795–1803, Jun. 2021.

[22] B. Perabathini, K. Tummuri, A. Agrawal, and V. S. Varma, "Efficient 3D placement of UAVs with QoS assurance in ad hoc wireless networks," in *Proc. 28th Int. Conf. Comput. Commun. Netw. (ICCCN)*, Jul. 2019, pp. 1–6.

[23] D. Ma, Y. Li, X. Hu, H. Zhang, and X. Xie, "An optimal three-dimensional drone layout method for maximum signal coverage and minimum interference in complex pipeline networks," *IEEE Trans. Cybern.*, vol. 52, no. 7, pp. 5897–5907, Jul. 2022.

[24] H. Kurunathan, K. Li, W. Ni, E. Tovar, and F. Dressler, "Deep reinforcement learning for persistent cruise control in UAV-aided data collection," in *Proc. IEEE 46th Conf. Local Comput. Netw. (LCN)*, Oct. 2021, pp. 347–350.

[25] A. A. Raja, H. Pervaiz, S. A. Hassan, S. Garg, M. S. Hossain, and M. J. Piran, "Coverage analysis of mmWave and THz-enabled aerial and terrestrial heterogeneous networks," *IEEE Trans. Intell. Transp. Syst.*, vol. 23, no. 11, pp. 22478–22491, Nov. 2022.

[26] M. Nafees, J. Thompson, and M. Safari, "Multi-tier variable height UAV networks: User coverage and throughput optimization," *IEEE Access*, vol. 9, pp. 119684–119699, 2021.

[27] M. M. U. Chowdhury, S. J. Maeng, E. Bulut, and I. Güvenç, "3-D trajectory optimization in UAV-assisted cellular networks considering antenna radiation pattern and backhaul constraint," *IEEE Trans. Aerosp. Electron. Syst.*, vol. 56, no. 5, pp. 3735–3750, Oct. 2020.

[28] Z. Yang, W. Xu, and M. Shikh-Bahaei, "Energy efficient UAV communication with energy harvesting," *IEEE Trans. Veh. Technol.*, vol. 69, no. 2, pp. 1913–1927, Feb. 2020.

[29] H. Zhang, J. Zhang, and K. Long, "Energy efficiency optimization for NOMA UAV network with imperfect CSI," *IEEE J. Sel. Areas Commun.*, vol. 38, no. 12, pp. 2798–2809, Dec. 2020.

[30] R. Masroor, M. Naeem, and W. Ejaz, "Efficient deployment of UAVs for disaster management: A multi-criterion optimization approach," *Comput. Commun.*, vol. 177, pp. 185–194, Sep. 2021.

[31] H. Mei, K. Yang, Q. Liu, and K. Wang, "Joint trajectory-resource optimization in UAV-enabled edge-cloud system with virtualized mobile clone," *IEEE Internet Things J.*, vol. 7, no. 7, pp. 5906–5921, Jul. 2020.

[32] C.-H. Liu, K.-H. Ho, and J.-Y. Wu, "mmWave UAV networks with multi-cell association: Performance limit and optimization," *IEEE J. Sel. Areas Commun.*, vol. 37, no. 12, pp. 2814–2831, Dec. 2019.

[33] M. M. Azari, F. Rosas, and S. Pollin, "Cellular connectivity for UAVs: Network modeling, performance analysis, and design guidelines," *IEEE Trans. Wireless Commun.*, vol. 18, no. 7, pp. 3366–3381, Jul. 2019.

[34] B. Galkin, J. Kibilda, and L. A. DaSilva, "Coverage analysis for low-altitude UAV networks in urban environments," in *Proc. IEEE Global Commun. Conf. (GLOBECOM)*, Dec. 2017, pp. 1–6.

[35] I. Mohammed, I. B. Collings, and S. V. Hanly, "Line of sight probability prediction for UAV communication," in *Proc. IEEE Int. Conf. Commun. Workshops (ICC Workshops)*, Jun. 2021, pp. 1–6.

[36] M. Gapeyenko, D. Moltchanov, S. Andreev, and R. W. Heath Jr., "Line-of-sight probability for mmWave-based UAV communications in 3D urban grid deployments," *IEEE Trans. Wireless Commun.*, vol. 20, no. 10, pp. 6566–6579, Oct. 2021.
[37] I. Mohammed, "Unmanned aerial vehicle communications: Channel modelling and deployment," Ph.D. thesis, Macquarie Univ., Sydney, NSW, Australia, Dec. 2021.

IMRAN MOHAMMED (Student Member, IEEE) received the B.Tech. degree in electrical and electronics engineering from the Rajiv Gandhi University of Knowledge Technologies (RGUKT), Nuzvid, in 2015, the M.Tech. degree in electrical engineering from the Indian Institute of Technology (IIT) Kanpur, in 2017, and the M.Res. degree from Macquarie University, Sydney, in 2018. He is currently pursuing the Ph.D. degree with the School of Engineering, Macquarie University, Sydney, Australia.

His research interests include optimization, localization, and UAV deployment analysis.

SWAROOP GOPALAM (Member, IEEE) received the B.Tech. degree in electrical engineering from the Indian Institute of Technology (IIT) Bombay, in 2014, and the M.Res. and Ph.D. degrees in engineering from Macquarie University, Sydney, Australia, in 2017 and 2021, respectively.

Since 2021, he has been a Research Fellow with the School of Engineering, Macquarie University. His research interests include resource allocation in wireless networks and the design of distributed and low-complexity algorithms.

IAIN B. COLLINGS (Fellow, IEEE) received the Ph.D. degree in systems engineering from The Australian National University, in 1995. He is currently a Professor with the School of Engineering, Macquarie University, Sydney, Australia. Previously, he spent nine years with the CSIRO, where he held a number of roles, including the Deputy Chief of Division, the Research Program Leader, and the Theme Leader, and nine years with The University of Melbourne and The University of Sydney. He has published more than 300 papers in the areas of wireless communications. He was a recipient of the Engineers Australia IREE Neville Thiele Award, in 2009, and the IEEE CommSoc Stephen O. Rice Award, in 2011. He has served as an Editor for IEEE TRANSACTIONS ON WIRELESS COMMUNICATIONS.

STEPHEN V. HANLY (Fellow, IEEE) received the Ph.D. degree in mathematics from Cambridge University, U.K., in 1994. He is currently a Professor with the School of Engineering, Macquarie University, Sydney, Australia. His research interest includes wireless communications. He was a recipient of the INFOCOM Best Paper Award, the IEEE Information Theory Society Award, the IEEE Communication Society Joint Paper Award, and the IEEE Communications Society Tutorial Paper Award. He has been an Associate Editor of the IEEE TRANSACTIONS ON WIRELESS COMMUNICATIONS and the Guest Editor of the IEEE JOURNAL ON SELECTED AREAS IN COMMUNICATIONS. He has taken major roles at several IEEE conferences and workshops, including IEEE ISIT and IEEE CTW.